communications biology

Article

https://doi.org/10.1038/s42003-024-06810-5

Lysosomal TMEM106B interacts with galactosylceramidase to regulate myelin lipid metabolism

Hideyuki Takahashi[1], Azucena Perez-Canamas[1], Chris W. Lee[2,3,4], Hongping Ye[5], Xianlin Han[5,6] & Stephen M. Strittmatter[1]

TMEM106B is an endolysosomal transmembrane protein not only associated with multiple neurological disorders including frontotemporal dementia, Alzheimer's disease, and hypomyelinating leukodystrophy but also potentially involved in COVID-19. Additionally, recent studies have identified amyloid fibrils of C-terminal TMEM106B in both aged healthy and neurodegenerative brains. However, so far little is known about physiological functions of TMEM106B in the endolysosome and how TMEM106B is involved in a wide range of human conditions at molecular levels. Here, we performed lipidomic analysis of the brain of TMEM106B-deficient mice. We found that TMEM106B deficiency significantly decreases levels of two major classes of myelin lipids, galactosylceramide and its sulfated derivative sulfatide. Subsequent co-immunoprecipitation assay showed that TMEM106B physically interacts with galactosylceramidase. We also found that galactosylceramidase activity was significantly increased in TMEM106B-deficient brains. Thus, our results suggest that TMEM106B interacts with galactosylceramidase to regulate myelin lipid metabolism and have implications for TMEM106B-associated diseases.

TMEM106B, which encodes TMEM106B, a highly glycosylated type II transmembrane protein, was initially identified as a risk modifier of frontotemporal lobar degeneration (FTLD) especially in patients with mutations in the *GRN* (FTLD-*GRN*)[1–3]. Subsequently, *TMEM106B* has also been linked to many other neurodegenerative diseases, such as Alzheimer's disease (AD)[4–6], chronic traumatic encephalopathy[7], and limbic-predominant age-related TDP-43 encephalopathy[8]. In addition, a de novo mutation in *TMEM106B* was found in patients with hypomyelinating leukodystrophy (HLD), a neurodevelopmental disorder characterized by myelin deficits[9]. Outside the brain, previous studies using an in vivo genetic screen have identified *TMEM106B* as a primary robust driver of lung cancer metastasis[10,11]. Furthermore, three different studies using genome-wide CRISPR screens independently identified TMEM106B as a host factor in certain cell lines for SARS-CoV-2, a strain of coronavirus that caused coronavirus disease 2019 (COVID-19)[12–14].

While *TMEM106B* has been shown to be associated with a great variety of human conditions, little is known about molecular mechanism by which TMEM106B is involved in those conditions. TMEM106B is localized at the endolysosome and thought to regulate several aspects of lysosomal function, but so far, a limited number of the interacting proteins have been reported[1,2]. Previous studies using cryo-electron microscopy have shown that truncated C-terminal TMEM106B forms amyloid fibrils in the brain[15–19]. However, the TMEM106B fibrils have been found not only in the brains of people with neurodegenerative diseases but also in neurologically normal ageing brains. Additionally, a disease-protective variant of TMEM106B also forms the amyloid fibrils. Although an increase in C-terminal TMEM106B fragment was biochemically detected in the sarkosyl-insoluble fraction of the brain of *TMEM106B* FTLD-risk SNP carriers, such an increase has not been observed in histological analysis[20–22]. It thus remains unclear whether the TMEM106B amyloid fibrils are involved in and responsible for the progression of TMEM106B-associated neurological disorders.

Dysregulation of lipid metabolism has been reported in the brains of FTLD-*GRN* patients as well as mouse models of FTLD-*GRN*[23–26]. Given the role of *TMEM106B* in FTLD-*GRN*, these findings raise a possibility that TMEM106B also regulates lipid metabolism under physiological and/or pathological conditions. Here, we performed lipidomic analysis of the brain

[1]Cellular Neuroscience, Neurodegeneration, Repair, Departments of Neurology and of Neuroscience, Yale University School of Medicine, New Haven, CT, 06536, USA. [2]Biomedical Research Institute of New Jersey (BRInj), Cedar Knolls, NJ, 07927, USA. [3]MidAtlantic Neonatology Associates (MANA), Morristown, NJ, 07960, USA. [4]Atlantic Health System, Morristown, NJ, 07960, USA. [5]Barshop Institute for Longevity and Aging Studies, University of Texas Health Science Center At San Antonio, San Antonio, TX, 78229, USA. [6]Department of Medicine, University of Texas Health Science Center At San Antonio, San Antonio, TX, 78229, USA. e-mail: stephen.strittmatter@yale.edu

of TMEM106B-deficient mice. We found that levels of two major classes of myelin lipids galactosylceramide (GalCer) and sulfatide (ST) are significantly reduced in TMEM106B-deficient brains. Subsequent unbiased proteomics and co-immunoprecipitation (co-IP) assay showed that TMEM106B physically interacts with galactosylceramidase (GALC), a lysosomal enzyme that hydrolyzes GalCer. We also found that GALC activity was significantly increased in TMEM106B-deficient brains. These results suggest that TMEM106B interacts with GALC to regulate myelin lipid metabolism particularly GalCer and ST levels. Thus, GALC inhibition may be a therapeutic target for TMEM106B-associated diseases.

Results

Levels of GalCer and ST are decreased in TMEM106B-deficient brains

Given the potential roles of TMEM106B in regulating lipid metabolism, we performed multidimensional mass spectrometry-based shotgun lipidomic analysis[27] using the brain of 12-month-old TMEM106B-deficient mice and wild-type (WT) littermates ($n = 6$, cohort 1). Lipid classes quantified in this discovery analysis include phosphatidylcholine (PC), phosphatidylethanolamine (PE), phosphatidylserine (PS), phosphatidylglycerol (PG), phosphatidylinositol (PI), phosphatidic acid (PA), cardiolipin (CL), lyso-phosphatidylcholine (LPC), lyso-phosphatidylethanolamine (LPE), lyso-cardiolipin (LCL), sphingomyelin (SM), ceramide (Cer), sulfatide (ST), hexosylceramide (HexCer), free cholesterol (CHL), cholesterol esters (CE), bis(monoacylglycerol)phosphate (BMP), and the total number of lipid species analyzed is 294 (Fig. 1a). Strikingly, with $p < 0.05$ cut off, we found that levels of multiple species of HexCer and ST were significantly decreased in TMEM106B-deficient brains (Fig. 1b, c), although TMEM106B deficiency affected levels of several species of other lipid classes such as PA, PE, and PC as well (Fig. 1c). Importantly, total levels of ST, HexCer, and PA but not the other classes were also found to be decreased in TMEM106B-deficient brains (Fig. 1d).

In our discovery analysis quantifying 294 lipid species, q-values were more than 0.05 even in the top differentially regulated lipid species (Supplementary Data 1). Therefore, to exclude the possibility that differences we observed in the discovery analysis are type I errors, we performed a replication analysis focusing on ST and HexCer using another cohort of 12-month-old TMEM106B-deficient mice and their WT littermates ($n = 7$, cohort 2). In the replication analysis, we observed a significant decrease in levels of most ST and HexCer species in TMEM106B-deficient brains (Fig. 2a, b), consistent with the discovery analysis. Total levels of ST and HexCer were also found to be significantly decreased in the cohort 2 of TMEM106B-deficient brains. Combining the cohorts 1 and 2, the p-values in differences between WT and TMEM106B-deficient brains in total ST and HexCer levels were less than 0.0001. Similar results were obtained between males and females (Fig. 2c, d). We thus concluded that a decrease in ST and HexCer is reproducibly observed irrespective of sex in TMEM106B-deficient brains.

HexCer comprises galactosylceramide (GalCer) and glucosylceramide (GlcCer). To determine levels of GalCer and GlcCer species separately, we next performed supercritical fluid chromatography-tandem mass spectrometry (SFC-MS/MS) using the brain homogenates from the cohort 1 and found that levels of multiple species of GalCer were significantly decreased in TMEM106B-deficient brains while none of GlcCer species was significantly altered (Figs. 1a and 3a, b). TMEM106B deficiency also significantly decreased total levels of GalCer but not GlcCer in the brain (Fig. 3c, d). Given that *TMEM106B* is an HLD gene, a decrease in GalCer and its sulfated derivative ST in TMEM106B-deficient brains was of particular interest as GalCer and ST are two major classes of myelin lipids[28]. Note that TMEM106B deficiency however had no effects on levels of Cer and SM (Fig. 1d), revealing a specific effect of TMEM106B deficiency on GalCer and ST levels. Together, our lipidomic data suggest that TMEM106B deficiency affects myelin lipid metabolism by decreasing levels of GalCer and ST in the brain.

TMEM106B physically interacts with GALC

To examine the mechanisms by which TMEM106B deficiency affects myelin lipid metabolism, we next sought to identify protein interaction partners of TMEM106B in the brain by using immunoprecipitation (IP) and liquid chromatography tandem mass spectrometry (LC-MS/MS) procedure (Fig. 4a). We confirmed that our anti-TMEM106B antibody cross-linked to protein A Sepharose beads reproducibly immunoprecipitated endogenous TMEM106B from mouse brains (Fig. 4b). Consistent with previous studies[29–31], we observed a ~70 kDa immunoreactive band of TMEM106B likely due to its glycosylation and homodimerization when the samples were run under non-reducing conditions (without 2-mercaptoethanol and heat). The ~70 kDa band was detected by two different anti-TMEM106B antibodies (Supplementary Fig. 1a).

LC-MS/MS analysis of elution of anti-TMEM106B immunoprecipitates identified 22 potential lysosomal TMEM106B-binding proteins. Of importance, some of them were previously reported to interact with TMEM106B, such as adapter protein subunits, vacuolar-ATPase V0 domain subunits, and cathepsin D[29,31,32], which validates the specificity of our IP and LC-MS/MS analysis (Fig. 4c). We also confirmed interaction between TMEM106B and cathepsin D using co-IP using HEK293T cells transfected with TMEM106B and cathepsin D (Supplementary Fig. 1b, c). Interestingly, one of the TMEM106B-binding proteins identified was galactosylceramidase (GALC), an enzyme that hydrolyzes GalCer (Fig. 4c, d). To confirm the results of MS analysis, we first performed co-IP assay using HEK293T cells transiently expressing myc-tagged GALC and green fluorescent protein (GFP), full-length (FL) TMEM106B-GFP, ΔC-TMEM106B-GFP, or ΔN-TMEM106B-GFP (Fig. 4e). We found that myc-tagged GALC was significantly co-immunoprecipitated with FL TMEM106B-GFP or ΔN-TMEM106B-GFP, but not GFP or ΔC-TMEM106B-GFP (Fig. 4e–g). Immunofluorescent analysis showed that ΔC-TMEM106B-GFP was localized at LAMP1-positive lysosomes in HEK293T cells, indicating that a decrease in co-immunoprecipitation of GALC by ΔC-TMEM106B-GFP is not due to loss of lysosomal localization by deletion of the C-terminal region (Supplementary Fig. 2). These results suggest that TMEM106B interacts with GALC in the lysosomal lumen. We also detected co-immunoprecipitation of myc-tagged GALC with immunoprecipitated endogenous TMEM106B in HEK293T cells, excluding the requirement for overexpression of two proteins or TMEM106B-GFP fusion protein (Supplementary Fig. 1d, e). T185S and D252N mutations in TMEM106B are associated with human FTLD and HLD, respectively[1]. These mutations however have no significant effects on co-IP of GALC (Supplementary Fig. 3).

TMEM106B regulates GALC activity

To further examine whether TMEM106B regulates GALC activity, we performed GALC activity assay using several brain regions of WT and TMEM106B-deficient mice. GALC activity can be measured using the fluorogenic substrate 4-methylumbelliferyl β-D-galactopyranoside (MUGAL) in the presence of $AgNO_3$, which specifically inhibits β-galactosidase (β-Gal)[33]. We found that GALC activity was significantly increased in the forebrain and brainstem but not cerebellum of TMEM106B-deficient mice (Fig. 5a), although TMEM106B expression was not markedly different between the brain regions and was slightly higher in the cerebellum of WT mouse brains (Supplementary Fig 4). We also performed GALC activity assay using 6-hexadecanoylamino-4-methylumbelliferyl-β-D-galactopyranoside (HMGal), a specific substrate for GALC[34], and obtained a similar result using the same forebrain lysates (Fig. 5b, c).

To examine whether TMEM106B deficiency affects protein levels of GALC, we homogenized brainstems from WT and TMEM106B-deficient mice using Tris-buffered saline with 0.4% digitonin and performed immunoblot analysis using an anti-mouse GALC antibody (CL1021AP)[35]. Increased GALC activity was confirmed in the digitonin-soluble brainstem lysates from TMEM106B-deficient mice (Fig. 5d). In the immunoblot analysis, we observed a mature GALC band at ~50 kDa in the brainstem

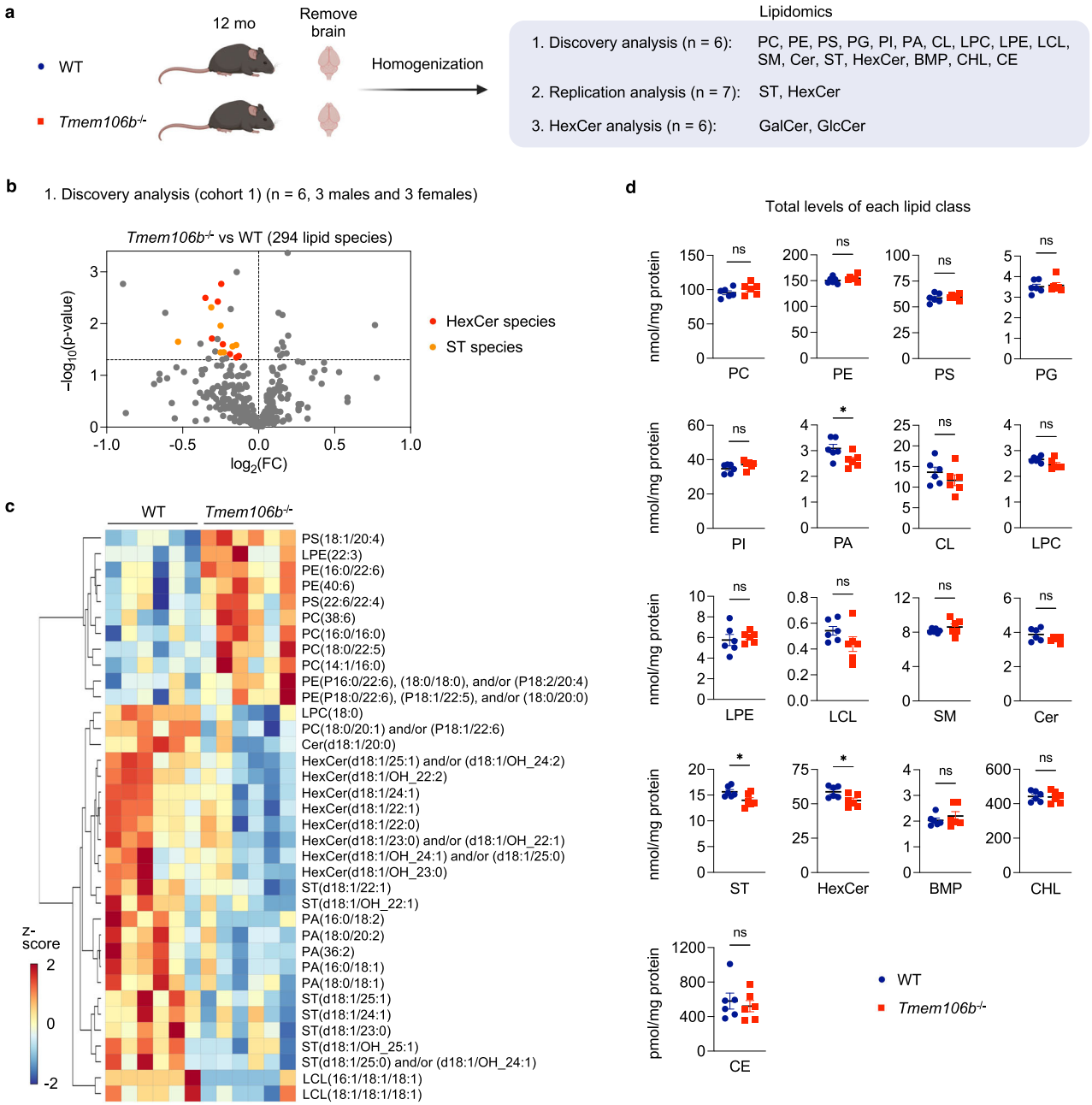

Fig. 1 | Hexosylceramide and sulfatide are decreased in TMEM106B-decifient brains. a Diagram showing the experimental procedures of lipidomic analysis using the brain of 12-month-old WT and *Tmem106b*$^{-/-}$ mice. First, targeted shotgun lipidomics were performed using 6 mice per genotype (cohort 1) to analyze 17 general lipid classes; phosphatidylcholine (PC), phosphatidylethanolamine (PE), phosphatidylserine (PS), phosphatidylglycerol (PG), phosphatidylinositol (PI), phosphatidic acid (PA), cardiolipin (CL), lyso-phosphatidylcholine (LPC), lyso-phosphatidylethanolamine (LPE), lyso-cardiolipin (LCL), sphingomyelin (SM), ceramide (Cer), sulfatide (ST), hexosylceramide (HexCer), free cholesterol (CHL), cholesterol esters (CE), bis(monoacylglycerol)phosphate (BMP). The total number of lipid species analyzed in this study is 294. Second, ST and HexCer levels were analyzed using another cohort with 7 mice per genotype (cohort 2) to test replicability. Finally, SFC-MS/MS was performed using cohort 1 to analyze galactosylceramide (GalCer) and glucosylceramide (GlcCer) species separately. The diagram was created with BioRender.com. **b** Volcano plot of discovery analysis with cohort 1 showing all 294 molecular lipid species. $n = 6$ (3 males and 3 females) per genotype. HexCer and ST species ($p < 0.05$) are highlighted in red and orange, respectively. The horizontal line indicates $p = 0.05$. p Values were calculated using two-tailed unpaired t-test. **c** Heatmap of all lipid species significantly affected by TMEM106B deficiency at $p < 0.05$ cutoff. **d** Scatter plots of the sum of all species within a lipid class for each class in WT versus *Tmem106b*$^{-/-}$. Mean ± SEM, $n = 6$ (3 males and 3 females) per genotype. *$p = 0.0411$ (PA), *$p = 0.0311$ (ST), *$p = 0.0279$ (HexCer); two-tailed unpaired t-test.

lysates but not in the negative control brain lysate from the twitcher mouse, which does not express GALC protein due to the presence of homozygous p.W339X genotype[36]. However, TMEM106B deficiency had no significant effects on the level of the mature GALC (Fig. 5e, f). Together, these results suggest that TMEM106B regulates enzymatic activity of GALC but not protein levels of mature GALC in the forebrain and brainstem.

Discussion

The major finding of the present study is that endolysosomal protein TMEM106B regulates myelin lipid metabolism. Our shotgun lipidomics and subsequent SFC-MS/MS revealed that levels of two major classes of myelin lipids GalCer and ST, which together constitute ~27% of the myelin lipid[28], were significantly decreased in the brain of TMEM106B-deficient

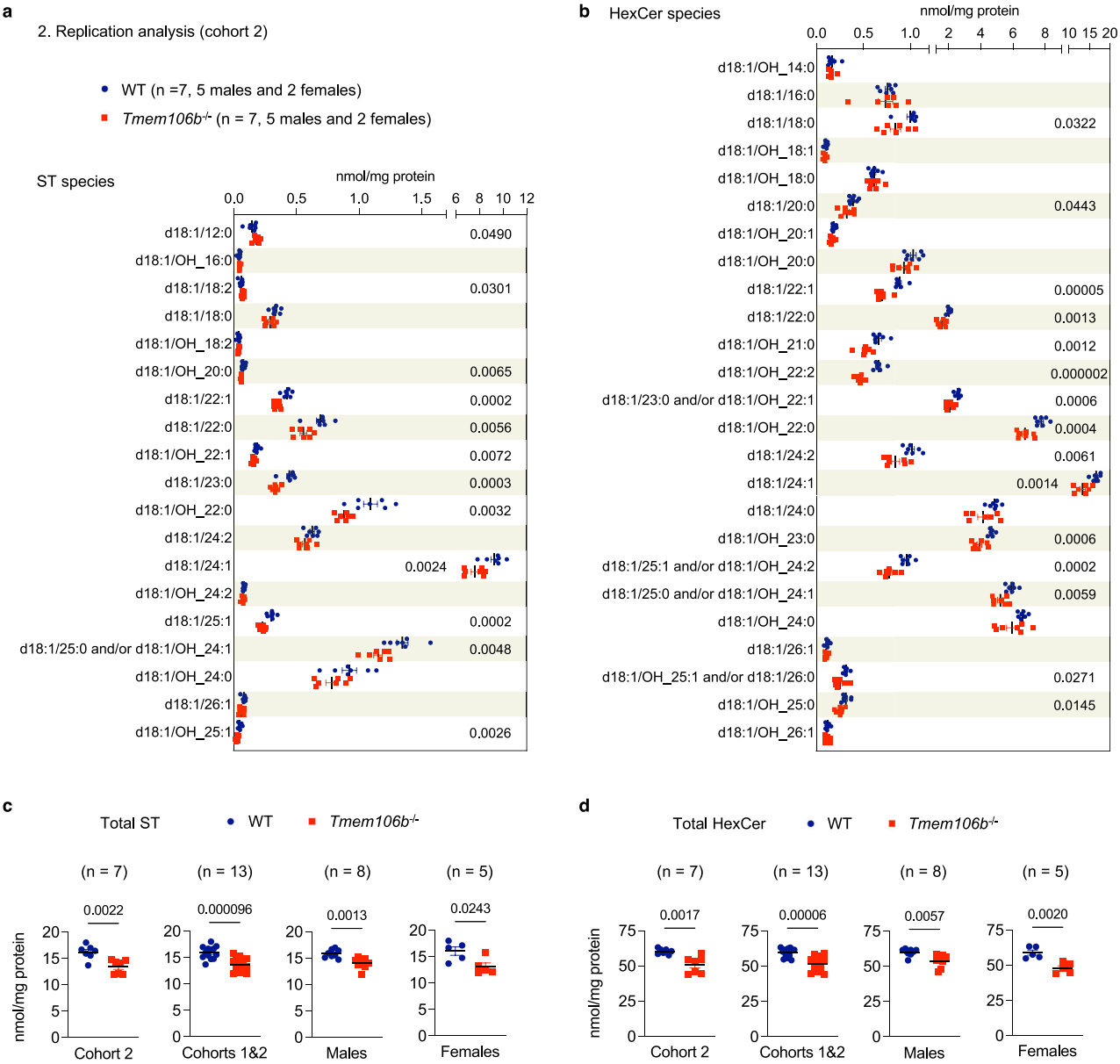

Fig. 2 | A decrease in HexCer and ST is also observed in another cohort of TMEM106B-deficient brains. a Levels of ST species in the brain of WT and *Tmem106b*$^{-/-}$ mice (cohort 2) at 12 months of age. Mean ± SEM, $n = 7$ mice (5 males and 2 females) per genotype. *p*-Values were determined using two-tailed unpaired *t*-test and shown on the right side of the graph when $p < 0.05$. **b** Levels of HexCer species in the brain of WT and *Tmem106b*$^{-/-}$ mice (cohort 2) at 12 months of age. Mean ± SEM, $n = 7$ mice (5 males and 2 females) per genotype. *p*-Values were determined using two-tailed unpaired *t*-test and shown on the right side of the graph when $p < 0.05$. **c** Total ST levels (sum of all species) in the brain of WT and *Tmem106b*$^{-/-}$ mice at 12 months of age. Mean ± SEM. Cohorts 1 and 2 are from the discovery and replication analyses, respectively. *p*-Values were determined using two-tailed unpaired *t*-test and were shown on the top of the graphs. **d** Total HexCer levels (sum of all species) in the brain of WT and *Tmem106b*$^{-/-}$ mice at 12 months of age. Mean ± SEM. Cohorts 1 and 2 are from the discovery and replication analyses, respectively. *p*-Values were determined using two-tailed unpaired *t*-test and were shown on the top of the graphs.

mice. Our results could potentially explain how a mutation in lysosomal TMEM106B leads to HLD. Importantly, dysfunction of myelin and/or myelin lipid metabolism has also been reported in other TMEM106B-associated brain disorders such as FTLD and AD. A recent study has shown disrupted myelin lipid metabolism in FTLD-*GRN* patients[25]. White matter abnormality has long been known in AD[37–42]. In addition, several studies have reported a significant reduction in ST levels in preclinical AD cases[43–46]. Interestingly, a previous rodent study has revealed that adult-onset ST deficiency is sufficient to cause AD-like neuroinflammation and cognitive impairment[47]. ST has also been shown to bind with high affinity to TREM2, a microglial AD risk factor[48]. These studies raise an intriguing possibility that the TMEM106B variant may be involved in the brain disorders by altering levels of GalCer and ST. Outside the brain, TMEM106B has been identified as a driver of lung cancer metastasis[10,11] and as a proviral host factor for SARS-CoV-2, a coronavirus that caused the COVID19 pandemic[12–14]. It will be interesting to examine whether a reduction in GalCer or ST is also observed in other TMEM106B-deficient tissues and protects against the lung cancer metastasis or SARS-CoV-2 infection.

In addition to GalCer and ST, TMEM106B deficiency has been shown to affect levels of other lipids such as PA and several species of PC and PE in our lipidomic analysis. How TMEM106B deficiency affects other lipids and whether those lipids are involved in TMEM106B-associated diseases remain

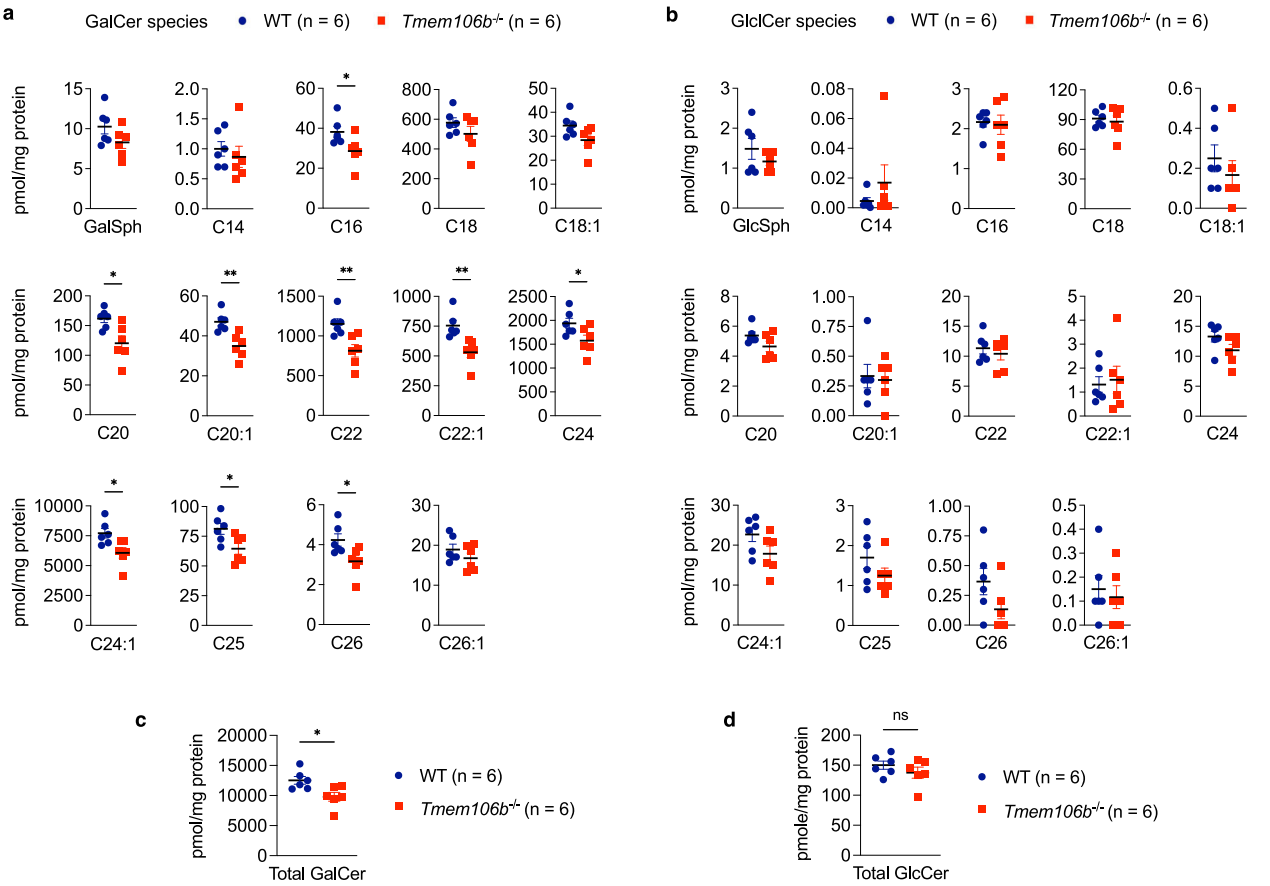

Fig. 3 | GalCer but not GlcCer is decreased in TMEM106B-deficient brains. **a** Levels of GalCer species in the brain of WT and *Tmem106b*$^{-/-}$ mice at 12 months of age. Mean ± SEM, $n = 6$ mice (3 males and 3 females) per genotype. $^{*}p = 0.0396$ (C16-GalCer), $^{*}p = 0.015$ (C20-GalCer), $^{**}p = 0.0034$ (C20:1-GalCer), $^{**}p = 0.0073$ (C22-GalCer), $^{**}p = 0.005$ (C22:1-GalCer), $^{*}p = 0.0423$ (C24-GalCer), $^{*}p = 0.0203$ (C24:1-GalCer), $^{*}p = 0.0285$ (C25-GalCer), $^{*}p = 0.0298$ (C26-GalCer); Two-tailed unpaired *t*-test. **b** Levels of GlcCer species in the brain of WT and *Tmem106b*$^{-/-}$ mice at 12 months of age. Mean ± SEM, $n = 6$ mice (3 males and 3 females) per genotype. None of the species were significantly affected by two-tailed unpaired *t*-test. **c** Total GalCer levels (sum of all species) in the brain of WT and *Tmem106b*$^{-/-}$ mice at 12 months of age. Mean ± SEM, $n = 6$ mice (3 males and 3 females) per genotype. $^{*}p = 0.0188$; two-tailed unpaired *t*-test. **d** Total GlcCer levels (sum of all species) in the brain of WT and *Tmem106b*$^{-/-}$ mice at 12 months of age. Mean ± SEM, $n = 6$ mice (3 males and 3 females) per genotype. Two genotypes were not significantly different by two-tailed unpaired *t*-test.

unclear. Several previous studies including ours have found that PGRN deficiency results in alteration in the levels of BMP, glucosylshingosine (GlcSph), GlcCer, and/or gangliosides in human and/or mouse models of FTLD-*GRN*[23,24,49]. However, these lipids were not significantly altered in TMEM106B-deficient brains. On the other hand, our previous lipidomic analysis has also revealed a decrease in some species of ST in PGRN-deficient brains[49], similar to the results of TMEM106B-deficient brains. Alteration in ST levels has been also reported in carriers of *TMEM106B* disease risk allele[21] as well as FTD-*GRN* cases[25]. Further work will be required to better understand our lipidomic results and link them to previous findings and ultimately to understand how *TMEM106B* is involved in multiple brain disorders including FTD-*GRN*.

Our unbiased IP and LC-MS/MS analysis identified GALC, an enzyme that hydrolyzes GalCer, as an interaction partner for TMEM106B. We also found that TMEM106B deficiency causes an increase in enzymatic activity of GALC while having no significant effect on its protein levels. It thus appears that TMEM106B binds and regulates activity of GALC in the lysosomal lumen, which explains reduced levels of both GalCer and ST in TMEM106B-deficient brains as ST is produced by sulfation of GalCer through the action of cerebroside sulfotransferase[50]. Future studies will have to determine whether TMEM106B directly associates with GALC as it is possible that the interaction observed in the co-IP is mediated by other proteins in the same physical complex. Although the T185 variant and D252N mutation in TMEM106B have been associated with FTLD and HLD, respectively[1], our co-IP assay showed no significant effects of the variant and mutation on TMEM106B binding to GALC. Whether the negative result is due to our assay system overexpressing both TMEM106B and GALC or whether the genetic variant and mutation influence activity of GALC rather than TMEM106B binding to GALC is currently unclear and requires further investigation. Recent cryo-electron microscopy studies found amyloid fibrils composed of C-terminal TMEM106B in human brains[15–18]. Our results suggest that the C-terminal fragment of TMEM106B could also interact with GALC. Effects of the C-terminal fragment on GALC activity in the brain will be an important avenue for future studies.

In the present study, we observed increased GALC activity in the forebrain and brainstem but not in the cerebellum of TMEM106B-deficient mice. The mechanism of the brain region-selective effect of TMEM106B on GALC activity is currently unclear. TMEM106B protein levels did not appear to be markedly different between these brain regions and are rather slightly increased in the cerebellum. Thus, lack of the effect from TMEM106B loss in the cerebellum is not simply explained by lower expression levels of TMEM106B in the cerebellum. Further investigation will be required to elucidate the exact mechanism.

In conclusion, accumulating evidence clearly suggests that lysosomal TMEM106B plays a key role in a wide range of human conditions. Our study revealed a physiological function of TMEM106B regulating myelin lipid metabolism by physically interacting with GALC. These findings provide mechanistic insights into TMEM106B-associated disorders and

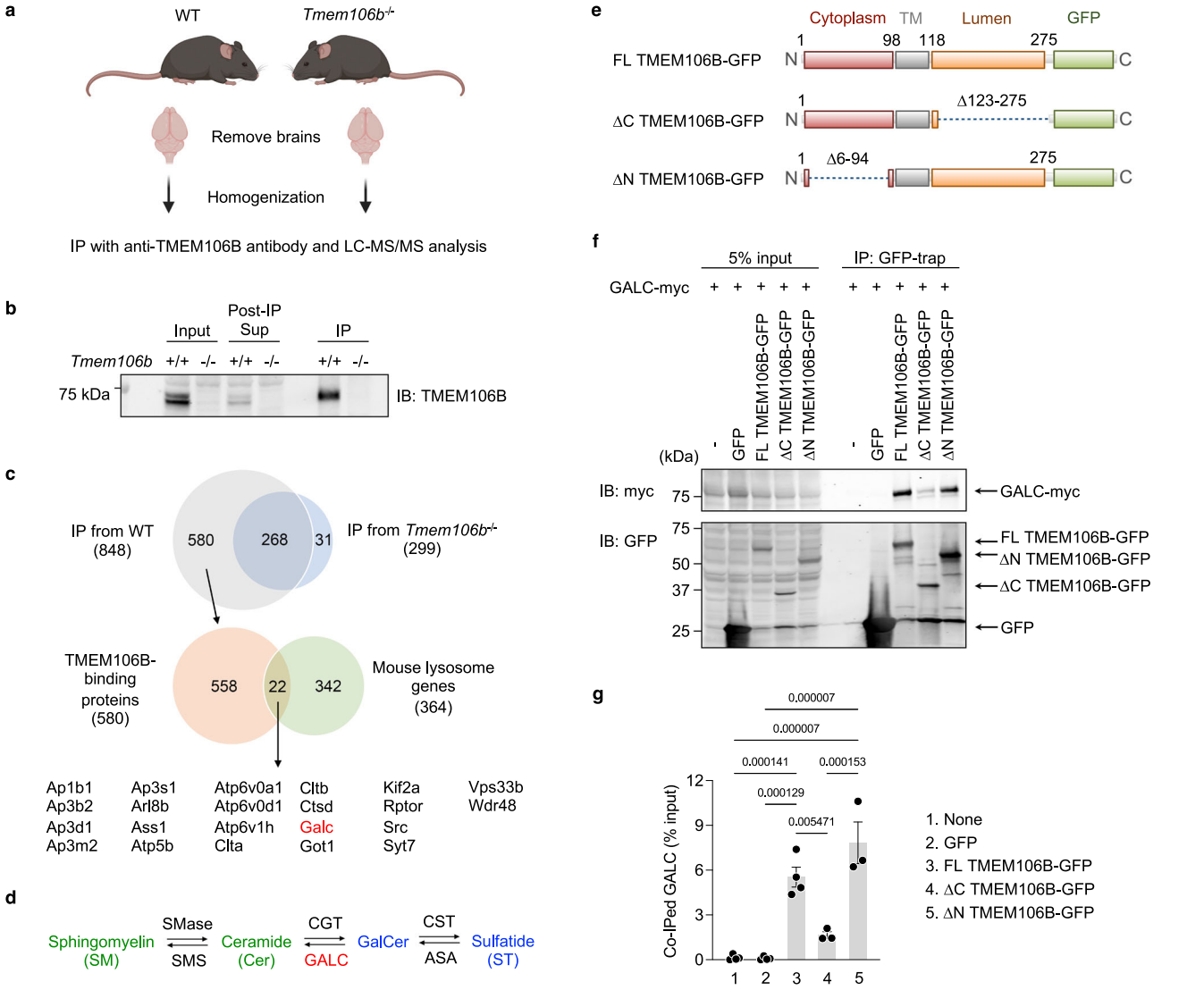

Fig. 4 | TMEM106B physically interacts with GALC via its luminal region. **a** Diagram showing experimental procedures of IP and LC-MS/MS analysis using mouse brains. The diagram was created with BioRender.com. **b** Representative blots to validate immunoprecipitation of endogenous TMEM106B from mouse brains using anti-TMEM106B antibody linked to protein A Sepharose. Note that all samples were run without treating with 2-mercaptoethanol and heat. **c** Venn diagrams to identify potential lysosomal TMEM106B-binding proteins. Total 848 proteins were identified in immunoprecipitates from WT brains but 268 of them were also found in those from TMEM106B-deficient brains. Thus, 580 proteins were considered as potential TMEM106B-binding proteins. Among them, 22 proteins were lysosomal proteins based on The Mouse Lysosomal Gene Database (http://lysosome.unipg.it/mouse.php). **d** Biosynthesis and degradation of GalCer and ST. SMase sphingomyelinase, SMS sphingomyelin synthase, CGT cerebroside galactosyl transferase, CST cerebroside sulfotransferase, ASA arylsulfatase A. TMEM106B deficiency results in a decrease in levels of GalCer and ST (blue) while having no effects on levels of Cer and SM (green). **e** Schematic drawing of full-length (FL) TMEM106B-GFP and TMEM106B-GFP lacking amino acids (aa)123–275 (ΔC) and aa6–94 (ΔN). **f** Representative blots of co-IP assays using HEK293T cells expressing GFP, FL TMEM106B-GFP, ΔC TMEM106B-GFP, or ΔN TMEM106B-GFP, together with myc-DDK-tagged mouse GALC. Note that all samples were treated with 2-mercaptoethanol and heat (95 °C) before running a gel. Monomeric TMEM106B-GFP fusion protein was detected at ~70 kDa (~43 kDa glycosylated TMEM106B + ~27 kDa GFP). **g** Quantification of co-IP in (**f**). Mean ± SEM, $n = 3$–4 experiments. p-Values were determined using one-way ANOVA with Tukey's multiple comparisons test and were shown on the top of the graph.

offer potential therapeutic strategies targeting TMEM106B-GALC interaction or modulating GalCer/ST levels.

Methods

Mouse strains

All animal protocols were approved by the Yale Institutional Animal Care and Use Committee. We have complied with all relevant ethical regulations for animal use. TMEM106B-deficient mice on C57BL/6 background were described previously[29]. This *Tmem106b*$^{-/-}$ line (*Tmem106b*$^{tm2a(KOMP)Wtsi}$) was generated by LacZ gene trap strategy and expresses 5–10% residual full-length TMEM106B protein[51,52]. All mice were housed in groups of 2–5 animals per cage with *ad libitum* access to standard mouse chow and water. Lighting was maintained at 12:12 light: dark cycle. Both male and female were used in this study and the numbers and ages are described in Figure legends.

Mouse brain tissue preparation

Mice were euthanized using CO_2. After transcardiac perfusion using ice-cold DPBS, the brains were removed, and the hemispheres were divided and stored at −80 °C until use. For GALC activity assay, forebrain and hindbrain were separated and the hindbrain was further dissected into cerebellum and brainstem. The dissected brain regions were snap-frozen in liquid nitrogen and stored at −80 °C until use.

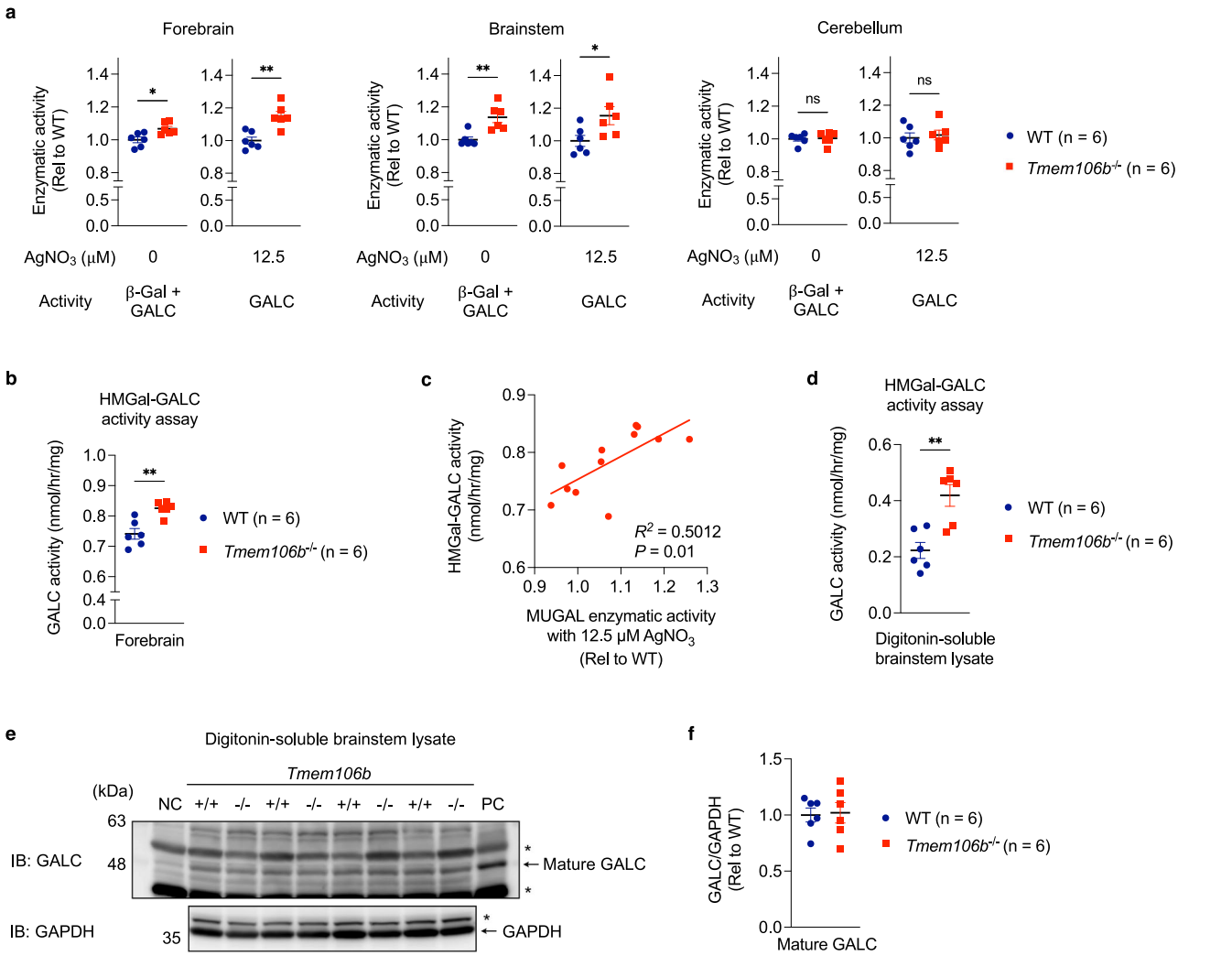

Fig. 5 | TMEM106B regulates GALC activity in the brain. a Enzymatic activity of forebrain, brainstem, and cerebellar extracts of WT and *Tmem106b*$^{-/-}$ mice at 13 months of age toward MUGAL substrate in the absent or presence of 12.5 μM $AgNO_3$. $n = 6$ mice (2 males and 4 females) per genotype. *$p = 0.0137$ (forebrain, 0 μM), **$p = 0.0016$ (forebrain, 12.5 μM), **$p = 0.0035$ (brainstem, 0 μM), *$p = 0.0383$ (brainstem, 12.5 μM); two-tailed unpaired *t*-test. **b** GALC activity of forebrain extracts of WT and *Tmem106b*$^{-/-}$ mice at 13 months of age measured using HMGal. $n = 6$ mice (2 males and 4 females) per genotype. **$p = 0.0017$; two-tailed unpaired *t*-test. **c** Correlation between the results of GALC activity assay using MUGAL and HMGal. **d** GALC activity of digitonin-soluble brainstem lysates of WT and *Tmem106b*$^{-/-}$ mice at 13 months of age measured with HMGal. $n = 6$ mice (2 males and 4 females) per genotype. **$p = 0.0022$; two-tailed unpaired *t*-test. **e** Representative blots of the digitonin-soluble brainstem lysates using anti-GALC and anti-GAPDH antibodies. The asterisks indicate non-specific bands. Whole brain lysates from ~40-day-old wild type and twitcher (GALC-deficient) mice were used as positive and negative controls (PC and NC). **f** Quantification of the blots in (**e**). Mean ± SEM, $n = 6$ mice (2 males and 4 females) per genotype. Two genotypes were not significantly different by two-tailed unpaired *t*-test.

Lipidomic analysis

Lipid species were analyzed using multidimensional mass spectrometry-based shotgun lipidomic analysis as previously described[49,53]. In brief, the brain hemispheres from 12-month-old TMEM106B-deficient mice and WT littermates were homogenized in 0.1× PBS and the brain homogenate containing 1.0 mg of protein, which was determined with a Pierce™ BCA protein assay kit (ThermoFisher SCIENTIFIC #23225), was transferred to a disposable glass culture test tube. A premixture of lipid internal standards was added prior to conducting lipid extraction for quantification of the targeted lipid species. The following internal standards purchased from Avanti Polar Lipids were used: 26.25 nmol of PC(14:1/14:1), 23.58 nmol of PE(16:1/16:1), 19.724 nmol of PS(14:0/14:0), 3.08 nmol of PG(15:0/15:0), 0.482 nmol of PA(14:0/14:0), 1.331 nmol of CL(14:0/14:0/14:0/14:0), 1.232 nmol of LPC(17:0), 1.257 nmol of LPE(14:0), 2.732 nmol of SM(d18:1/12:0), 1.053 nmol of Cer(d18:1/17:0), 3.08 nmol of ST(d18:0/16:0), 8.008 nmol of GalCer(d18:1/15:0), 169.33 nmol of d7-Cholesterol, 0.247 nmol of CE(18:1(d7)). PG(15:0/15:0) was also used for BMP and PI. CL(14:0/14:0/14:0/14:0) was also used for LCL. Lipid extraction was performed using a modified Bligh and Dyer procedure[53], and each lipid extract was reconstituted in chloroform:methanol (1:1, *v:v*) at a volume of 400 μL/mg protein. Phosphatidylethanolamine (PE) and cholesterol (CHL) were derivatized as described previously[54,55] before lipidomic analysis. Quantitative analysis of isomeric bis(monoacylglycerol)phosphate (BMP) and phosphatidylglycerol (PG) was performed as reported[56].

For shotgun lipidomics, lipid extract was further diluted to a final concentration of ~500= fmol total lipids per μL. Mass spectrometric analysis was performed on a triple quadrupole mass spectrometer (TSQ Altis, Thermo Fisher Scientific, San Jose, CA) and a Q Exactive mass spectrometer (Thermo Scientific, San Jose, CA), both of which were equipped with an automated nanospray device (TriVersa NanoMate, Advion Bioscience Ltd., Ithaca, NY) as previously described[57]. The triple quadrupole and orbitrap systems were run separately for mutual validation and identification. Identification and quantification of lipid species were performed using an automated software program as previously reported[58,59]. Data processing

(e.g., ion peak selection, baseline correction, data transfer, peak intensity comparison and quantitation) was performed as previously described[59]. The result was normalized to the protein content (nmol lipid/mg protein or pmol lipid/mg protein for CE). Total levels of each lipid class were determined by adding up the levels of all species of the class. Full results of lipidomic results are provided as Supplementary Data files.

GlcCer and GalCer species analysis separated by SFC-MS/MS

Separation of GlcCer and GalCer species was performed at the Lipidomics Shared Resource at Medical University of South Carolina. Lipids were extracted from the 0.1× PBS homogenate containing 1 mg of protein, and levels of GlcCer and GalCer species were measured with supercritical fluid chromatography-tandem mass spectrometry (SFC-MS/MS) analysis. The equipment consists of a Waters UPC^2 system coupled to a Thermo Scientific Quantum Access Max triple quadrupole mass spectrometer equipped with an ESI probe operating in the multiple reaction monitoring (MRM) positive ion mode tuned and optimized for the Waters UPC^2 system.

Chromatographic separations are obtained utilizing a carbon dioxide gas and methanol with 1 mM ammonium formate in 0.2% formic acid. Prior to analysis, samples undergo an ethyl acetate/isopropanol liquid-liquid extraction as previously described[60–62]. The quantitative analyses of GalCer and GlcCer are based on eight-point calibration curves generated for each target analyte as previously described[60–62]. The synthetic standards along with a set of internal standards are spiked into an artificial matrix; they are then subjected to an identical extraction procedure as the biological samples. These extracted standards are then analyzed by the SFC-MS/MS system. Peaks for the target analytes and internal standards are recorded and processed using the instrument's software. Plotting the analyte/internal standard peak area ratios against analyte concentrations generates the analyte specific calibration curves. Any glycosphingolipids for which no standards are available are quantitated using the calibration curve of its closest counterpart. Levels of GalCer and GlcCer species were expressed as picomoles per milligrams of protein. Total levels of GalCer or GlcCer were determined by adding up the levels of all species of GalCer or GlcCer. Full results of GalCer and GlcCer species analyses by SFC-MS/MS are provided as Supplementary Data files.

Immunoprecipitation

Immunoprecipitation using mouse brain lysates was performed as previously reported[52]. WT and *Tmem106b*$^{-/-}$ brains at 6–7-months of age were homogenized in ice-cold TBST (50 mM Tris-HCl, pH 7.4, 150 mM NaCl, 1% Triton X-100) supplemented with cOmplete-mini (Roche). After ultracentrifugation at 100,000 × *g*, the supernatant was pre-cleared using Protein A-Sepharose CL-4B (SIGMA #17-0780-01) for 3 h at 4 °C. Then, anti-TMEM106B antibody (Abcam #ab140185) covalently linked to Protein A-Sepharose CL-4B with BS^3 (ThermoScientific #21580) was added to the pre-cleared lysates. After overnight incubation at 4 °C, the immunoprecipitates were washed six times with ice-cold TBST and proteins were eluted with 2× Laemmli buffer (Bio-Rad).

In solution protein digestion

A methanol-chloroform precipitation was performed according to standard protocols. The protein pellet was resuspended in 20 µL 8 M urea, 0.4 M ammonium bicarbonate with vigorous vortexing. Proteins were reduced by the addition of 2.0 µL 45 mM dithiothreitol (ThermoFisher SCIENTIFIC #20290) and incubation at 37 °C for 30 min, and then alkylated with the addition of 2.0 µL 100 mM iodoacetamide (SIGMA #I1149) and incubation in the dark at room temperature for 30 min. The urea was diluted to 2 M by adding 55 µL of water. Samples were then enzymatically digested using 1.0 µL 0.5 mg/ml trypsin (Promega Seq. Grade Mod. Trypsin, # V5113) and incubation at 37 °C for 16 h. Digestion was halted by acidification with trifluoroacetic acid (TFA) to 0.1%. The mixtures were desalted using C18 Ultra microspin columns (The Nest Group, #SUM SS18V) following the manufacturer's directions. Peptides were eluted with 2 × 160 µL 0.1% TFA, 80% acetonitrile, then speedvaced dry. Peptides were dissolved in 32 µL MS loading buffer (2% aceotonitrile, 0.2% trifluoroacetic acid). A nanodrop measurement (Thermo Scientific Nanodrop 2000 UV–Vis Spectrophotometer) determined protein concentrations (A260/A280). Each sample was then further diluted with MS loading buffer to 0.04 µg/µL, with 200 ng (5 µL) injected for LC–MS/MS analysis.

LC–MS/MS on the Thermo Scientific Q Exactive Plus

LC–MS/MS analysis was performed on a Thermo Scientific Q Exactive Plus equipped with a Waters nanoAcquity UPLC system utilizing a binary solvent system (A: 100% water, 0.1% formic acid; B: 100% acetonitrile, 0.1% formic acid). Trapping was performed at 5 µL/min, 97% Buffer A for 3 min using a Waters Symmetry® C18 180 µm × 20 mm trap column. Peptides were separated using an ACQUITY UPLC PST (BEH) C18 nanoACQUITY Column 1.7 µm, 75 µm × 250 mm (37 °C) and eluted at 300 nL/min with the following gradient: 3% buffer B at initial conditions; 5% B at 1 min; 35% B at 90 min; 50% B at 105 min; 90% B at 110 min, 90% B at 115 min; return to initial conditions at 116 min. MS was acquired in profile mode over the 300-1,700 m/z range using 1 microscan, 70,000 resolution, AGC target of 3E6, and a maximum injection time of 45 ms. Data dependent MS/MS were acquired in centroid mode on the top 20 precursors per MS scan using 1 microscan, 17,500 resolution, AGC target of 1E5, maximum injection time of 100 ms, and an isolation window of 1.7 m/z. Precursors were fragmented by HCD activation with a collision energy of 28%. MS/MS were collected on species with an intensity threshold of 2E4, charge states 2-6, and peptide match preferred. Dynamic exclusion was set to 20 s.

Peptide identification

Data was analyzed using Proteome Discoverer (version 1.3) software and searched in-house using the Mascot algorithm (version 2.6.0) (Matrix Science). The data was searched against a SwissProtein database with taxonomy restricted to *Mus musculus*. Search parameters used were trypsin digestion with up to 2 missed cleavages; peptide mass tolerance of 10 ppm; MS/MS fragment tolerance of 0.02 Da; and variable modifications of methionine oxidation and carbamidomethyl cysteine. Normal and decoy database searches were run, with the confidence level was set to 95% ($p < 0.05$).

Co-immunoprecipitation (co-IP) using HEK293T cells

Co-IP was performed as previously reported[29,49] with slight modifications. Plasmids encoding myc-DDK-tagged mouse GALC (#MR225749) and human GALC (#RC211578), mouse cathepsin D (#MR225301) were purchased from OriGene Technologies, Inc. Plasmids encoding human TMEM106B-mCherry was generated using pmCherry-N1 vector (Clontech #632523). T185S and D252N mutations were introduced using Quik change II XL site-directed mutagenesis kit (Agilent #200521). Two days after transfection using Lipofectamine™ 2000 (ThermoFisher SCIENTIFIC #11668019), HEK293T cells were harvested and lysed with ice-cold 50 mM Tris-HCl pH 7.5, 150 mM NaCl, 1% Triton X-100 supplemented with cOmplete-mini and PhosSTOP (Roche). After ultracentrifugation at 100,000×*g* for 30 min at 4 °C, the supernatant was incubated with ChromoTek GFP- or RFP-trap® Agarose (proteintech #gta or #rta) for 3 h at 4 °C. For immunoprecipitation of endogenous TMEM106B, anti-TMEM106B (Cell Signaling Technology #93334) or Rabbit (DA1E) mAb IgG XP(R) Isotype Control (Cell Signaling Technology #3900) prebound to Protein A-Sepharose CL-4B was added to the supernatant and the samples were nutated for 5 h at 4 °C. The immunoprecipitates were washed five times with ice-cold lysis buffer and boiled with 2× Laemmli Buffer (Bio-Rad) with βME.

Immunoblot

Immunoblot was performed as previously reported[29,49,63], with slight modification. For the brain samples (except for Fig. 5e and Supplementary Fig. 1a), the Triton X-100-soluble fraction was mixed with 2× Laemmli Sample Buffer (Bio-Rad #1610737) without adding βME and kept on ice

until running SDS-PAGE to detect ~70 kDa putative TMEM106B dimers. The protein samples were resolved by SDS-PAGE with precast 4–20% Tris-glycine gels (Bio-Rad #5671095) and transferred using an iBlot 2 Transfer Device onto nitrocellulose membranes (Invitrogen #IB23001). The membranes were incubated in blocking buffer (Rockland MB-070) for 1 h at room temperature and then incubated overnight at 4 °C in blocking buffer with primary antibodies: TMEM106B (Abcam #ab140185, 1:1000), TMEM106B (E7H7Z) (Cell Signaling Technology #93334, 1:1000), GFP (B-2) (Santa Cruz #sc-9996, 1:500), Myc-Tag (71D10) (Cell Signaling Technology #2278, 1:1000), Myc-Tag (9B11) (Cell Signaling Technology #2276, 1:1000), β-actin (8H10D10) (Cell Signaling Technology #3700, 1:2000), RFP Tag (RF5R) (ThermoFisher SCIENTIFIC #MA5-15257, 1:1000), β-tubulin (D3U1W) (Cell Signaling Technology #86298, 1:1000). The membranes were then washed three times with TBST for 3 min and incubated in secondary antibodies (Li-Cor, IR Dye 680 or 800, all 1:10,000) for 1 h at room temperature. After washing three times with TBST for 3 min, The immunoreactive protein bands were visualized with an Odyssey Infrared imaging system (Li-Cor) and quantified using Fiji (ImageJ) software.

Immunofluorescence

HEK293T cells were plated onto 8-well chamber slides (LAB-TEK, #154941) using DMEM (GIBCO #11965-092) supplemented with 10% fetal bovine serum (GIBCO #16000-044) and Pen Strep (GIBCO #15140-122) and cultured for one day before transfection. Two days after transfection using Lipofectamine™ 2000 (ThermoFisher SCIENTIFIC #11668019), transfected cells were fixed with 4% paraformaldehyde (SIGMA #158127) in DPBS for 1 h. After washing with DPBS, the cells were permeabilized and blocked with 10% normal donkey serum, 0.2% Triton X-100 in DPBS for 30 min and then incubated overnight at 4 °C with primary antibodies diluted in 1% normal donkey serum and 0.2% Triton X-100 in DPBS. Primary antibodies used were rabbit anti-LAMP1 antibody (Cell Signaling Technology #9091, 1:75) and mouse anti-GFP antibody (SantaCruz #sc-9996, 1:200). The cells were then washed three times with DPBS and incubated for 1.5 h at room temperature in Alexa Fluor 488 donkey anti-mouse IgG (H + L) (Invitrogen #A21202, 1:500) and Alexa Fluor 568 donkey anti-rabbit IgG (H + L) (Invitrogen #A10042, 1:500) in 1% normal donkey serum, 0.2% Triton X-100 in DPBS. After washing three times with DPBS, the chamber slides were coverslipped with VECTASHIELD antifade mounting medium with DAPI (VECTOR laboratories, #H-1200). Images were taken using LSM800 confocal microscopy (Zeiss) with 63× magnification objective lens. The maximal intensity projection function was used with z-stack confocal images.

GALC activity assay

GALC activity assay was performed as previously reported with modifications[33]. Briefly, frozen dissected brain tissues (forebrain, brainstem, and cerebellum) were homogenized using a dounce homogenizer in citrate/phosphate (CP) buffer pH 5.2, 1% Triton X-100, supplemented with cOmplete-mini and phosSTOP (Roche) on ice and incubated for 30 min at 4 °C. The supernatants after ultracentrifugation at 100,000 × *g* were used for GALC activity assay. Protein concentrations were determined by Pierce™ BCA protein assay kit (ThermoFisher SCIENTIFIC #23225) and used for normalization. Five micro litters of the supernatants were mixed and pre-incubated with 10 µL of H_2O (vehicle) or $AgNO_3$ (SIGMA #204390) (final concentration 12.5 µM) in CP buffer pH 4 in 96-well black plate (Costar #3916) for 10 min at room temperature (RT) and then added 30 µL of 4-methylumbelliferyl β-D-galactopyranoside (MUGAL) (final concentration 0.8 mM) (SIGMA #M1633) and incubated for 1 h at 37 °C. Reaction was stopped by adding 200 µL of 0.5 M glycine-NaOH pH 10.5. Measurements were taken with VICTOR Nivo® multimode plate reader (PerkinElmer) at excitation of 355 nm and emission of 460 nm.

Brain lysate preparation for HMGal-GALC assay and immunoblot

Mouse brainstem was homogenized in cold TDI buffer (TBS, 0.4% digitonin, protease inhibitors cocktail, pH 7.4) as a 20% (w/v) homogenate followed by centrifugation at 16,000 × *g* for 1 h at 4 °C. The supernatant was then separated from the detergent-insoluble fraction and analyzed for protein concentration by BCA protein assay.

HMGal-GALC activity assay

GALC activity in the brainstem supernatant was measured by a fluorescence substrate turnover assay as previously reported[34,64] with modifications. Fifty micrograms of total protein were added to a reaction cocktail containing CP buffer pH 4.5, 7 mg/ml sodium taurocholate, 2 mg/ml oleic acid and 0.5 mg/ml 6-hexadecanoylamino-4-methylumbelliferyl-β-D-galactopyranoside (HMGal; Biosynth Inc., Newbury, UK) and incubated for 2 h at 37 °C. The reaction was stopped by adding 2 volumes of 0.1 M glycine/0.1 M sodium hydroxide solution and 4 volumes of absolute ethanol. The concentration of reaction product was determined by fluorescence plate reader at excitation of 385 nm and emission of 450 nm. A 4-methylumbelliferone standard curve was ran in parallel for calculation of absolute GALC activity expressed in nmol per hour per milligram protein.

Immunoblot for GALC

Fifty micrograms of total protein from the brainstem supernatant were mixed with Tris-glycine sample buffer and reducing reagent followed by heating at 85 °C for 2 min. The samples were resolved by SDS-PAGE with 10–20% Tris-glycine gel (Thermofisher Scientific, Waltham, MA). Gel proteins were transferred to PVDF membranes by Criterion blotter (Bio-Rad, Hercules, CA) according to manufacturer's instruction. The protein blot was blocked in 5% non-fat milk for 2 h at room temperature followed by incubation with an anti-mouse GALC antibody (CL1021AP, 250 ng/ml)[35] for 18 h at 4 °C. The blot was probed with an anti-chicken IgY horseradish peroxidase-conjugated antibody (Millipore Sigma, Burlington, MA; 500 ng/ml) for 1 h at room temperature, followed by signal development using the Immobilon Western Chemiluminescent HRP substrate (MilliporeSigma, Burlington, MA). Western blot images were obtained by the Image-quant LAS 4000 mini system. To obtain the GAPDH signals, the GALC blots were washed extensively in TBST buffer (TBS, 0.05% tween-20, pH 7.4) then reprobed with an anti-GAPDH antibody (Proteintech #60004-1-Ig, 1:100,000) for 30 min at room temperature. After incubation with an anti-mouse IgG horseradish peroxidase-conjugated antibody (Millipore Sigma, 500 ng/ml) for 30 min at room temperature, the signal images were obtained by the same procedures as above. GALC protein levels were quantified by densitometric measurement of target band intensity normalized to GAPDH levels.

Statistics and reproducibility

Two-tailed unpaired *t* test (for 2 groups) and one-way ANOVA (for >2 groups) were performed using GraphPad Prism (version 9.2.0). All data are shown as mean ± SEM and specific *n* values are reported in each Figure legend. Data are considered to be statistically significant if $p < 0.05$. For lipidomic analysis, by using two independent mouse cohorts (i.e., discovery ($n = 6$) and replication ($n = 7$) cohorts), we confirmed that a decrease in HexCer and ST is consistently observed in TMEM106B-deficient brains. All lipidomic analyses were performed by investigators who were blinded to the genotypes. All co-IP experiments were independently repeated at least three time. All attempts at replication were successful. GALC activity of WT and TMEM106B-deficient brains was measured by two different assays (MUGAL and HMGal) and investigators and similar results were obtained.

Data availability

Uncropped blot images are provided as Supplementary Fig. 5 in the Supplementary Information. LC–MS/MS raw data for Fig. 3 have been deposited to the ProteomeXchange Consortium via the PRIDE partner repository with the dataset identifier PXD043192. Full results of the discovery, replication, and HexCer analyses of lipidomics are provided in the Supplementary Data 1–3, respectively. Source data are provided in Supplementary Data 4.

Received: 21 July 2023; Accepted: 30 August 2024;
Published online: 05 September 2024

References

1. Feng, T., Lacrampe, A. & Hu, F. Physiological and pathological functions of TMEM106B: a gene associated with brain aging and multiple brain disorders. *Acta Neuropathol.* **141**, 327–339 (2021).
2. Perneel, J. & Rademakers, R. Identification of TMEM106B amyloid fibrils provides an updated view of TMEM106B biology in health and disease. *Acta Neuropathol.* **144**, 807–819 (2022).
3. Van Deerlin, V. M. et al. Common variants at 7p21 are associated with frontotemporal lobar degeneration with TDP-43 inclusions. *Nat. Genet* **42**, 234–239 (2010).
4. Bellenguez, C. et al. New insights into the genetic etiology of Alzheimer's disease and related dementias. *Nat Genet.* https://doi.org/10.1038/s41588-022-01024-z (2022).
5. Wightman, D. P. et al. A genome-wide association study with 1,126,563 individuals identifies new risk loci for Alzheimer's disease. *Nat. Genet.* **53**, 1276–1282 (2021).
6. Hu, Y. et al. rs1990622 variant associates with Alzheimer's disease and regulates TMEM106B expression in human brain tissues. *BMC Med.* **19**, 11 (2021).
7. Cherry, J. D. et al. Variation in TMEM106B in chronic traumatic encephalopathy. *Acta Neuropathol. Commun.* **6**, 115 (2018).
8. Nelson, P. T. et al. Limbic-predominant age-related TDP-43 encephalopathy (LATE): consensus working group report. *Brain* **142**, 1503–1527 (2019).
9. Simons, C. et al. A recurrent de novo mutation in TMEM106B causes hypomyelinating leukodystrophy. *Brain* **140**, 3105–3111 (2017).
10. Kundu, S. T. et al. TMEM106B drives lung cancer metastasis by inducing TFEB-dependent lysosome synthesis and secretion of cathepsins. *Nat. Commun.* **9**, 2731 (2018).
11. Grzeskowiak, C. L. et al. In vivo screening identifies GATAD2B as a metastasis driver in KRAS-driven lung cancer. *Nat. Commun.* **9**, 2732 (2018).
12. Baggen, J. et al. Genome-wide CRISPR screening identifies TMEM106B as a proviral host factor for SARS-CoV-2. *Nat. Genet.* **53**, 435–444 (2021).
13. Schneider, W. M. et al. Genome-scale identification of SARS-CoV-2 and Pan-coronavirus host factor networks. *Cell* **184**, 120–132.e114 (2021).
14. Wang, R. et al. Genetic screens identify host factors for SARS-CoV-2 and common cold coronaviruses. *Cell* **184**, 106–119.e114 (2021).
15. Chang, A. et al. Homotypic fibrillization of TMEM106B across diverse neurodegenerative diseases. *Cell.* https://doi.org/10.1016/j.cell.2022.02.026 (2022).
16. Fan, Y. et al. Generic amyloid fibrillation of TMEM106B in patient with Parkinson's disease dementia and normal elders. *Cell Res.* **32**, 585–588 (2022).
17. Jiang, Y. X. et al. Amyloid fibrils in FTLD-TDP are composed of TMEM106B and not TDP-43. *Nature* **605**, 304–309 (2022).
18. Schweighauser, M. et al. Age-dependent formation of TMEM106B amyloid filaments in human brains. *Nature* **605**, 310–314 (2022).
19. Takahashi, H. & Strittmatter, S. M. An unexpected protein aggregate in diseased and ageing brains. *Nature* **605**, 227–228 (2022).
20. T Vicente, C. et al. C-terminal TMEM106B fragments in human brain correlate with disease-associated TMEM106B haplotypes. *Brain* **146**, 4055–4064 (2023).
21. Lee, J. Y. et al. The major TMEM106B dementia risk allele affects TMEM106B protein levels, fibril formation, and myelin lipid homeostasis in the ageing human hippocampus. *Mol. Neurodegener.* **18**, 63 (2023).
22. Marks, J. D. et al. TMEM106B core deposition associates with TDP-43 pathology and is increased in risk SNP carriers for frontotemporal dementia. *Sci. Transl. Med* **16**, eadf9735 (2024).
23. Logan, T. et al. Rescue of a lysosomal storage disorder caused by Grn loss of function with a brain penetrant progranulin biologic. *Cell* **184**, 4651–4668.e4625 (2021).
24. Boland, S. et al. Deficiency of the frontotemporal dementia gene GRN results in gangliosidosis. *Nat. Commun.* **13**, 5924 (2022).
25. Marian, O. C. et al. Disrupted myelin lipid metabolism differentiates frontotemporal dementia caused by GRN and C9orf72 gene mutations. *Acta Neuropathol. Commun.* **11**, 52 (2023).
26. Evers, B. M. et al. Lipidomic and Transcriptomic Basis of Lysosomal Dysfunction in Progranulin Deficiency. *Cell Rep.* **20**, 2565–2574 (2017).
27. Han, X. *Lipidomics: Comprehensive Mass Spectrometry of Lipids/Xianlin Han*. (John Wiley & Sons, Inc., Hoboken, New Jersey, 2016).
28. Marcus, J. & Popko, B. Galactolipids are molecular determinants of myelin development and axo-glial organization. *Biochim Biophys. Acta* **1573**, 406–413 (2002).
29. Klein, Z. A. et al. Loss of TMEM106B ameliorates lysosomal and frontotemporal dementia-related phenotypes in progranulin-deficient mice. *Neuron* **95**, 281–296.e286 (2017).
30. Chen-Plotkin, A. S. et al. TMEM106B, the risk gene for frontotemporal dementia, is regulated by the microRNA-132/212 cluster and affects progranulin pathways. *J. Neurosci.* **32**, 11213–11227 (2012).
31. Feng, T. et al. A role of the frontotemporal lobar degeneration risk factor TMEM106B in myelination. *Brain* **143**, 2255–2271 (2020).
32. Stagi, M., Klein, Z. A., Gould, T. J., Bewersdorf, J. & Strittmatter, S. M. Lysosome size, motility and stress response regulated by fronto-temporal dementia modifier TMEM106B. *Mol. Cell Neurosci.* **61**, 226–240 (2014).
33. Martino, S. et al. Specific determination of beta-galactocerebrosidase activity via competitive inhibition of beta-galactosidase. *Clin. Chem.* **55**, 541–548 (2009).
34. Wiederschain, G., Raghavan, S. & Kolodny, E. Characterization of 6-hexadecanoylamino-4-methylumbelliferyl-beta-D- galactopyranoside as fluorogenic substrate of galactocerebrosidase for the diagnosis of Krabbe disease. *Clin. Chim. Acta* **205**, 87–96 (1992).
35. Lee, W. C. et al. Molecular characterization of mutations that cause globoid cell leukodystrophy and pharmacological rescue using small molecule chemical chaperones. *J. Neurosci.* **30**, 5489–5497 (2010).
36. Lee, W. C. et al. Suppression of galactosylceramidase (GALC) expression in the twitcher mouse model of globoid cell leukodystrophy (GLD) is caused by nonsense-mediated mRNA decay (NMD). *Neurobiol. Dis.* **23**, 273–280 (2006).
37. Brun, A. & Englund, E. A white matter disorder in dementia of the Alzheimer type: a pathoanatomical study. *Ann. Neurol.* **19**, 253–262 (1986).
38. Migliaccio, R. et al. White matter atrophy in Alzheimer's disease variants. *Alzheimers Dement*. https://doi.org/10.1016/j.jalz.2012.04.010 (2012).
39. Bartzokis, G. et al. White matter structural integrity in healthy aging adults and patients with Alzheimer disease: a magnetic resonance imaging study. *Arch. Neurol.* **60**, 393–398, (2003).
40. Englund, E. Neuropathology of white matter changes in Alzheimer's disease and vascular dementia. *Dement. Geriatr. Cogn. Disord.* **9**, 6–12 (1998).
41. Stout, J. C., Jernigan, T. L., Archibald, S. L. & Salmon, D. P. Association of dementia severity with cortical gray matter and abnormal white matter volumes in dementia of the Alzheimer type. *Arch. Neurol.* **53**, 742–749 (1996).
42. Nasrabady, S. E., Rizvi, B., Goldman, J. E. & Brickman, A. M. White matter changes in Alzheimer's disease: a focus on myelin and oligodendrocytes. *Acta Neuropathol. Commun.* **6**, 22 (2018).
43. Han, X., D, M. H., McKeel, D. W. Jr., Kelley, J. & Morris, J. C. Substantial sulfatide deficiency and ceramide elevation in very early Alzheimer's disease: potential role in disease pathogenesis. *J. Neurochem.* **82**, 809–818 (2002).
44. Cheng, H., Wang, M., Li, J. L., Cairns, N. J. & Han, X. Specific changes of sulfatide levels in individuals with pre-clinical Alzheimer's disease: an early event in disease pathogenesis. *J. Neurochem.* **127**, 733–738 (2013).

45. Wallin, A., Gottfries, C. G., Karlsson, I. & Svennerholm, L. Decreased myelin lipids in Alzheimer's disease and vascular dementia. *Acta Neurol. Scand.* **80**, 319–323 (1989).
46. Han, X. et al. Cerebrospinal fluid sulfatide is decreased in subjects with incipient dementia. *Ann. Neurol.* **54**, 115–119 (2003).
47. Qiu, S. et al. Adult-onset CNS myelin sulfatide deficiency is sufficient to cause Alzheimer's disease-like neuroinflammation and cognitive impairment. *Mol. Neurodegener.* **16**, 64 (2021).
48. Wang, Y. et al. TREM2 lipid sensing sustains the microglial response in an Alzheimer's disease model. *Cell* **160**, 1061–1071 (2015).
49. Takahashi, H. et al. Reduced progranulin increases tau and alpha-synuclein inclusions and alters mouse tauopathy phenotypes via glucocerebrosidase. *Nat. Commun.* **15**, 1434 (2024).
50. Blomqvist, M., Zetterberg, H., Blennow, K. & Mansson, J. E. Sulfatide in health and disease. The evaluation of sulfatide in cerebrospinal fluid as a possible biomarker for neurodegeneration. *Mol. Cell Neurosci.* **116**, 103670 (2021).
51. Zhou, X. et al. Loss of Tmem106b exacerbates FTLD pathologies and causes motor deficits in progranulin-deficient mice. *EMBO Rep.* **21**, e50197 (2020).
52. Perez-Canamas, A., Takahashi, H., Lindborg, J. A. & Strittmatter, S. M. Fronto-temporal dementia risk gene TMEM106B has opposing effects in different lysosomal storage disorders. *Brain Commun.* **3**, fcaa200 (2021).
53. Wang, M. & Han, X. Multidimensional mass spectrometry-based shotgun lipidomics. *Methods Mol. Biol.* **1198**, 203–220 (2014).
54. Han, X., Yang, K., Cheng, H., Fikes, K. N. & Gross, R. W. Shotgun lipidomics of phosphoethanolamine-containing lipids in biological samples after one-step in situ derivatization. *J. Lipid Res.* **46**, 1548–1560 (2005).
55. Cheng, H., Jiang, X. & Han, X. Alterations in lipid homeostasis of mouse dorsal root ganglia induced by apolipoprotein E deficiency: a shotgun lipidomics study. *J. Neurochem.* **101**, 57–76 (2007).
56. Wang, M., Palavicini, J. P., Cseresznye, A. & Han, X. Strategy for quantitative analysis of isomeric bis(monoacylglycero)phosphate and phosphatidylglycerol species by shotgun lipidomics after one-step methylation. *Anal. Chem.* **89**, 8490–8495 (2017).
57. Han, X., Yang, K. & Gross, R. W. Microfluidics-based electrospray ionization enhances the intrasource separation of lipid classes and extends identification of individual molecular species through multi-dimensional mass spectrometry: development of an automated high-throughput platform for shotgun lipidomics. *Rapid Commun. Mass Spectrom.* **22**, 2115–2124 (2008).
58. Wang, M., Wang, C., Han, R. H. & Han, X. Novel advances in shotgun lipidomics for biology and medicine. *Prog. Lipid Res.* **61**, 83–108 (2016).
59. Yang, K., Cheng, H., Gross, R. W. & Han, X. Automated lipid identification and quantification by multidimensional mass spectrometry-based shotgun lipidomics. *Anal. Chem.* **81**, 4356–4368 (2009).
60. Bielawski, J., Szulc, Z. M., Hannun, Y. A. & Bielawska, A. Simultaneous quantitative analysis of bioactive sphingolipids by high-performance liquid chromatography-tandem mass spectrometry. *Methods* **39**, 82–91 (2006).
61. Bielawski, J. et al. Comprehensive quantitative analysis of bioactive sphingolipids by high-performance liquid chromatography-tandem mass spectrometry. *Methods Mol. Biol.* **579**, 443–467 (2009).
62. Bielawski, J. et al. Sphingolipid analysis by high performance liquid chromatography-tandem mass spectrometry (HPLC-MS/MS). *Adv. Exp. Med Biol.* **688**, 46–59 (2010).
63. Takahashi, H. et al. Opposing effects of progranulin deficiency on amyloid and tau pathologies via microglial TYROBP network. *Acta Neuropathol.* **133**, 785–807 (2017).
64. Iacono, D. et al. Galactosylceramidase deficiency and pathological abnormalities in cerebral white matter of Krabbe disease. *Neurobiol. Dis.* **174**, 105862 (2022).

Acknowledgements

We thank Kristin DeLuca for assistance with mouse husbandry. We also thank Dr. Janet Deane of University of Cambridge for helpful discussion. This work was supported by National Institute on Aging of the National Institutes of Health under grant number R01AG034924 and R01AG066165 to S.M.S. We also thank the MS & Proteomics Resource at Yale University for providing the necessary mass spectrometers and the accompany biotechnology tools funded in part by the Yale School of Medicine and by the Office of The Director, National Institutes of Health (S10OD02365101A1, S10OD019967, and S10OD018034). This work was supported in part by the Lipidomics Shared Resource, Hollings Cancer Center, Medical University of South Carolina (P30 CA138313 and P30 GM103339). This work was also supported by a grant from National Institute on Aging (RF1 AG061729) to X.H. The content is solely the responsibility of the authors and does not necessarily represent the official views of the National Institutes of Health.

Author contributions

H.T. and S.M.S. planned and oversaw all aspects of the study. H.T. performed IP using the mouse brain, subsequent co-IP, and GALC activity assay using MUGAL and analyzed the results of most of the experiments in this study. A.P.-C. performed mouse breeding and prepared all brain samples used in lipidomics. C.W.L. performed GALC activity assay using HMGal and immunoblot using anti-GALC antibody. H.Y. and X.H. performed discovery and replication lipidomic analyses. H.T. and S.M.S. wrote the paper with input and revisions from all authors.

Competing interests

The authors declare no competing interests.

Additional information

Supplementary information The online version contains supplementary material available at https://doi.org/10.1038/s42003-024-06810-5.

Correspondence and requests for materials should be addressed to Stephen M. Strittmatter.

Peer review information *Communications Biology* thanks the anonymous reviewers for their contribution to the peer review of this work. Primary Handling Editor: Manuel Breuer.